Scientific Research Publishing

Journal of Applied Mathematics and Physics, 2024, 12, 3638-3654
https://www.scirp.org/journal/jamp
ISSN Online: 2327-4379
ISSN Print: 2327-4352

Hybrid Nanofluid Flow over a Stretching Curved Surface with Induced Magnetic Field and Homogeneous-Heterogeneous Reactions

Ming Shen[1], Yunhua Zheng[1], Yihong Liu[1], Hui Chen[2*], Mengchen Zhang[1]

[1]School of Mathematics and Statistics, Fuzhou University, Fuzhou, China
[2]School of Mechanical Engineering and Automation, Fuzhou University, Fuzhou, China
Email: *felixceng@fzu.edu.cn

How to cite this paper: Shen, M., Zheng, Y.H., Liu, Y.H., Chen, H. and Zhang, M.C. (2024) Hybrid Nanofluid Flow over a Stretching Curved Surface with Induced Magnetic Field and Homogeneous-Heterogeneous Reactions. *Journal of Applied Mathematics and Physics*, **12**, 3638-3654.
https://doi.org/10.4236/jamp.2024.1210218

Received: October 15, 2024
Accepted: October 28, 2024
Published: October 31, 2024

Abstract

This study explores the 2D stretching flow of a hybrid nanofluid over a curved surface influenced by a magnetic field and reactions. A steady laminar flow model is created with curvilinear coordinates, considering thermal radiation, suction, and magnetic boundary conditions. The nanofluid is made of water with copper and MWCNTs as nanoparticles. The equations are transformed into nonlinear ODEs and solved numerically. The model's accuracy is confirmed by comparing it with published data. Results show that fluid velocity increases, temperature decreases, and concentration increases with the curvature radius parameter. The hybrid nanofluid is more sensitive to magnetic field changes in velocity, while the nanofluid is more sensitive to magnetic boundary coefficient changes. These insights can optimize heat and mass transfer in industrial processes like chemical reactors and wastewater treatment.

Keywords

Hybrid Nanofluids, Stretching Curved Surface, Induced Magnetic Field, Improved Shooting Method

1. Introduction

The pursuit of more efficient heat transfer technologies has been a key driver for advancements across various industries [1] [2], from energy production to medical applications. Nanofluids [3], which incorporate nanoscale solid particles into base fluids, have emerged as a promising candidate to tackle the challenge of overcoming the thermal limitations of conventional fluids. Nanoparticles demonstrate

significant potential to enhance the thermal performance of fluids[4] due to their exceptional thermal conductivity, which paves the way for the development of more efficient heat transfer systems. Consequently, nanofluid technology is widely regarded as a promising and highly potential technical solution. However, existing single nanofluids have limitations in terms of stability and convective heat transfer performance under high-temperature conditions [5]. To overcome these challenges, researchers are actively investigating the potential of hybrid nanofluids, aiming to leverage their combined properties to achieve superior heat transfer performance [6]-[9].

In recent years, an increasing number of researchers have begun to focus on how the dynamic behavior of homogeneous-heterogeneous reactions affects fluid flow and heat transfer characteristics, providing new directions for optimizing reaction processes and improving system efficiency. Chaudhary *et al.* [10] [11] developed a simplified model of stagnation point boundary layer flow for homogeneous-heterogeneous reactions, analyzing the steady-state behavior of the system when the diffusion coefficients of the reactants and autocatalysts are equal and unequal. Inayat *et al.* [12] explored the flow of three-dimensional nanofluids over a stretching surface, focusing on the heat transfer caused by melting as well as the effects of homogeneous and heterogeneous reactions. Kotha *et al.* [13] investigated the flow of thermoradiative viscoelastic fluids with homogeneous and heterogeneous chemical reactions in a helical coil, finding that the regularized L.R. method yielded the best results.

The fluid flow induced by a curved stretching sheet has garnered significant interest from researchers because of its applications in the engineering of stretchable elastic materials. Maria *et al.* [14] studied homogeneous-heterogeneous reactions in two-dimensional MHD radiative flow caused by a curved stretching surface. Maryiam *et al.* [15] investigated the influence of homogeneous-heterogeneous reactions on the MHD peristaltic mechanism of Ellis fluid in a curved channel. Sanni *et al.* [16] investigated the steady MHD viscous flow over a nonlinear quadratic stretching surface. Additionally, they [17] examined the two-dimensional heat transfer of a conductive cross fluid over a power-law stretching surface under the influence of a variable external magnetic field.

In recent years, a new technology called liquid gating has emerged, considered one of the top ten emerging technologies in the chemical field in 2020 by the International Union of Pure and Applied Chemistry [18]. Sheng *et al.* [19] demonstrated that external magnetic fields can precisely control the collective dynamics of confined magnetic colloids. Additionally, experiments have shown a strong link between the threshold pressure for fluid invasion and magnetic field strength [20]. Chen *et al.* [21] designed a new boundary condition with the magnetic response to study superior heat and mass transfer of Maxwell ternary nanofluid for a stagnation-point flow.

Upon reviewing the existing literature on fluid flow research, it is evident that the utilization of curvilinear coordinate systems remains relatively scarce. In light

of this, our study aims to delve into the impact of homogeneous-heterogeneous reactions and induced magnetic fields on the flow, heat transfer, and mass transfer properties of binary nanofluids within a curvilinear coordinate framework. Additionally, we will examine the effects of permeable surfaces and magnetic-responsive boundaries on these characteristics, thereby contributing to a more comprehensive understanding of fluid dynamics in complex geometries.

Nomenclature

κ	Thermal conductivity ($W \cdot m^{-1} \cdot K^{-1}$)	q_r	Radiative heat flux parameter ($kg \cdot s^{-3}$)
C_p	Specific heat ($J \cdot kg^{-1} \cdot K^{-1}$)	Re_s	Local Reynolds number
Q	Volumetric rate of heat source ($W \cdot m^{-3}$)	Nu	Local Nusselt number
T_∞	Ambient temperature (K)	k	Dimensionless curvature radius parameter
T_w	Surface temperature (K)	***Greek symbols***	
D_A, D_B	Diffusion coefficient ($m^2 \cdot s^{-1}$)	μ_{ef}	Magnetic permeability ($kg \cdot ms^{-2} \cdot A^{-2}$)
A, B	Chemical species	ρ	Density ($kg \cdot m^{-3}$)
C_0	Reference concentration (dimensionless) ($kg \cdot m^{-3}$)	μ	Dynamic viscosity ($kg \cdot m^{-1} \cdot s^{-1}$)
s_0	Suction/injection velocity ($m \cdot s^{-1}$)	ζ	Magnetic diffusivity ($m^2 \cdot s^{-1}$)
h_0	Latent magnetic induction strength (Am^{-1})	δ	Ratio of diffusion coefficients
p	Pressure	ϑ_f	Kinematic viscosity ($m^2 \cdot s^{-1}$)
K^*	Mean absorption coefficient (m^{-1})	τ_c, τ_s	Rate constants
a	Stretching constant (s^{-1})	τ_1, τ_2	Homogeneous/Heterogeneous reaction parameter
M_0	Constant upstream magnetic field (Am^{-1})	σ^*	Stefan-Boltzmann constant ($Wm^{-2} \cdot K^{-4}$)
M_e	Free magnetic density (Am^{-1})	β	Magnetic field parameter
R_d	Thermal radiation	ϕ_1	Volume fraction of Cu
D	Heat generation parameter	ϕ_2	Volume fraction of MWCNTs
Sc	Schmidt number	ϕ	Volume fraction of nanoparticles
f	Dimensionless velocity	η	Dimensionless distance
g	Dimensionless IMF	θ	Dimensionless temperature
P	Dimensionless pressure	***Subscripts***	
Pr_M	Prandtl magnetic number	bf	Base fluid
Pr	Prandtl number	s_1	Cu nanoparticle
G, H	Dimensionless concentration	s_2	MWCNTs nanoparticle
S	Suction ($S > 0$)/injection ($S < 0$) parameter	nf	Nanofluid
h	Coefficient of magnetic boundary	hnf	Ternary nanofluid
C_f	Skin friction coefficient		

2. Mathematical Analysis

2.1. Modeling Assumptions

The curvilinear coordinates (r, s) are employed for our analysis, where r represents the radial distance from the center O of the curved geometry, and s signifies the arc length component aligned with the flow direction. The surface is stretched with velocity ($u_w(s) = as$) along the s-direction, as displayed in **Figure 1**. An induced magnetic field M is also taken into account, with M_1 and M_2 denoting the parallel and normal components, respectively.

In the analysis of the homogeneous and heterogeneous reactions, two chemical species, denoted A and B, are taken into account. The homogeneous reaction, following cubic autocatalysis, is expressed as

$$A + 2B \to 3B, \text{ rate} = \tau_c C_1 C_2^2,$$

while the heterogeneous reaction, occurring on the catalyst surface can be described as

$$A \to B, \text{ rate} = \tau_s C_1.$$

Here τ_c and τ_s are the rate constants, while the concentrations of chemical species A and B are denoted as C_1 and C_2, respectively.

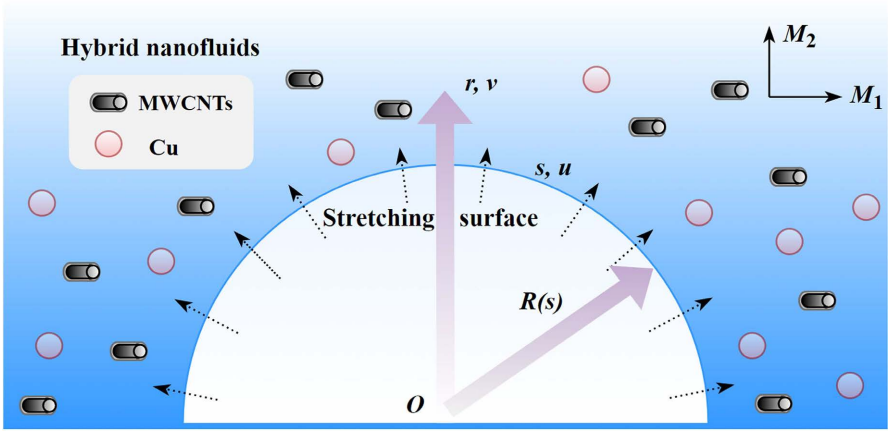

Figure 1. Physical configuration and coordinate system.

2.2. Govern Equations

Under the above assumptions and in the presence of thermal radiation according to Rosseland's approximation [22], ignoring free charges and the displacement currents, the governing boundary layer equations for the flow, induced magnetic field, energy and concentration equations in curvilinear coordinates can be stated as [23]:

$$\frac{\partial}{\partial r}\{(r+R)v\} + R\frac{\partial u}{\partial s} = 0, \tag{2.1}$$

$$\frac{u^2}{r+R} = \frac{1}{\rho_{hnf}}\frac{\partial p}{\partial r}, \tag{2.2}$$

$$\begin{aligned} & v\frac{\partial u}{\partial r}+\frac{Ru}{r+R}\frac{\partial u}{\partial s}+\frac{uv}{r+R} \\ & =-\frac{1}{\rho_{hnf}}\frac{R}{r+R}\frac{\partial p}{\partial s}+\frac{\mu_{hnf}}{\rho_{hnf}}\left(\frac{\partial^2 u}{\partial r^2}+\frac{1}{r+R}\frac{\partial u}{\partial r}-\frac{u}{(r+R)^2}\right) \\ & +\frac{\mu_{ef}}{4\pi\rho_{hnf}}\left(\frac{R}{r+R}M_1\frac{\partial M_1}{\partial s}+\frac{M_1M_2}{r+R}+M_2\frac{\partial M_1}{\partial r}\right), \end{aligned} \tag{2.3}$$

$$\frac{\partial}{\partial r}\left\{(r+R)M_2\right\}+R\frac{\partial M_1}{\partial s}=0, \tag{2.4}$$

$$\begin{aligned} & \frac{R}{r+R}u\frac{\partial M_1}{\partial s}+v\frac{\partial M_1}{\partial r}+\frac{uM_2}{r+R}-\left[\frac{R}{r+R}M_1\frac{\partial u}{\partial s}+M_2\frac{\partial u}{\partial r}+\frac{M_1v}{r+R}\right] \\ & =\zeta\left(\frac{\partial^2 M_1}{\partial r^2}+\frac{1}{r+R}\frac{\partial M_1}{\partial r}-\frac{M_1}{(r+R)^2}\right), \end{aligned} \tag{2.5}$$

$$\begin{aligned} \left(\frac{R}{r+R}u\frac{\partial T}{\partial s}\right)+v\frac{\partial T}{\partial r} & =\left(\frac{\kappa_{hnf}}{(\rho C_p)_{hnf}}+\frac{16\sigma^* T_\infty^{\ 3}}{3K^*(\rho C_p)_{hnf}}\right)\left(\frac{\partial^2 T}{\partial r^2}+\frac{1}{r+R}\frac{\partial T}{\partial r}\right) \\ & +\frac{Q}{(\rho C_p)_{hnf}}(T-T_\infty), \end{aligned} \tag{2.6}$$

$$\frac{R}{r+R}u\frac{\partial C_1}{\partial s}+v\frac{\partial C_1}{\partial r}=D_A\left\{\frac{\partial^2 C_1}{\partial r^2}+\frac{1}{r+R}\frac{\partial C_1}{\partial r}\right\}-\tau_c C_1C_2^2 \tag{2.7}$$

$$\frac{R}{r+R}u\frac{\partial C_2}{\partial s}+v\frac{\partial C_2}{\partial r}=D_B\left\{\frac{\partial^2 C_2}{\partial r^2}+\frac{1}{r+R}\frac{\partial C_2}{\partial r}\right\}+\tau_c C_1C_2^2 \tag{2.8}$$

with the following boundary conditions

$$u=u_w(s)=as, \tag{2.9}$$

$$v=-s_0-h_0\frac{sgn(s_0)\mu_{ef}}{4\pi a^2 s^2\rho_{hnf}}M_1^{\ 2}(s,0), \tag{2.10}$$

$$T=T_w,\ M_2=0,\ \frac{\partial M_1}{\partial r}=0, \tag{2.11}$$

$$D_A\frac{\partial C_1}{\partial r}=\tau_s C_1,\ D_B\frac{\partial C_2}{\partial r}=-\tau_s C_1\ \text{ at } r=0, \tag{2.12}$$

$$u\to 0,\ \frac{\partial u}{\partial r}\to 0,\ T\to T_\infty,\ \text{ as } r\to\infty \tag{2.13}$$

$$M_1\to M_e(s),\ C_1\to C_0,\ C_2\to 0\ \text{ as } r\to\infty. \tag{2.14}$$

Taking into account the profound influence of the magnetic response boundary on the alteration of flow dynamics, the boundary condition (2.10) is designated as the magnetically responsive condition. In the event that h_0 equals zero, this condition reduces to the conventional velocity boundary condition, which encompasses both suction phenomena.

Considering the distinct geometries of the selected nanoparticles, the expressions for thermal-physical properties of hybrid nanofluids are listed in **Table 1**.

Table 1. Thermal-physical properties of hybrid nanofluids.

Properties	Hybrid nanofluids
Dynamic Viscosity	$\frac{\mu_{nf}}{\mu_f}=\frac{1}{(1-\phi)^{2.5}}$ $\frac{\mu_{hnf}}{\mu_f}=\frac{1}{(1-\phi_1)^{2.5}(1-\phi_2)^{2.5}}=A_1$
Density	$\frac{\rho_{nf}}{\rho_f}=(1-\phi)+\phi\frac{\rho_s}{\rho_f}$ $\frac{\rho_{hnf}}{\rho_f}=(1-\phi_2)\left[1-\left(1-\frac{\rho_{s1}}{\rho_f}\right)\phi_1\right]+\phi_2\frac{\rho_{s2}}{\rho_f}=A_2$
Heat Capacity	$\frac{(\rho C_p)_{nf}}{(\rho C_p)_f}=(1-\phi)+\phi\frac{(\rho C_p)_s}{(\rho C_p)_f}$ $\frac{(\rho C_p)_{hnf}}{(\rho C_p)_f}=(1-\phi_2)\left\{1-\phi_1+\phi_1\frac{(\rho C_p)_{s_1}}{(\rho C_p)_f}\right\}+\phi_2\frac{(\rho C_p)_{s_2}}{(\rho C_p)_f}=A_3$
Thermal Conductivity	$\frac{\kappa_{nf}}{\kappa_f}=\frac{\kappa_s+2\kappa_f-2\phi(\kappa_f-\kappa_s)}{\kappa_s+2\kappa_f+\phi(\kappa_f-\kappa_s)}$ $\frac{\kappa_{hnf}}{\kappa_{bf}}=\frac{\kappa_{s_2}+2\kappa_{bf}-2\phi_2(\kappa_{bf}-\kappa_{s_2})}{\kappa_{s_2}+2\kappa_{bf}+\phi_2(\kappa_{bf}-\kappa_{s_2})}$ **Where** $\frac{\kappa_{bf}}{\kappa_f}=\frac{\kappa_{s1}+2\kappa_f-2\phi_1(\kappa_f-\kappa_{s1})}{\kappa_{s1}+2\kappa_f+\phi_1(\kappa_f-\kappa_{s1})}$ $\frac{\kappa_{hnf}}{\kappa_f}=A_4$

2.3. Normalization

To simplify the analysis, we apply the following similarity transformation:

$$\eta=\sqrt{\frac{a}{\vartheta_f}}r,\ u=asf'(\eta),\ v=-\frac{R}{r+R}\sqrt{a\vartheta_f}f(\eta), \tag{2.15}$$

$$p=\rho_f a^2 s^2 P(\eta),\ M_1=M_0 sg'(\eta), \tag{2.16}$$

$$M_2=-M_0\frac{R}{r+R}\sqrt{\frac{\vartheta_f}{a}}g(\eta),\ \theta(\eta)=\frac{T-T_\infty}{T_w-T_\infty}, \tag{2.17}$$

$$C_1=C_0G(\eta),\ C_2=C_0H(\eta). \tag{2.18}$$

The conservation equations for mass and the magnetic field, namely Equations (2.1) and (2.4), are satisfied identically under the previously mentioned transformation. Consequently, the governing equations are reduced to the following system of nonlinear coupled ordinary differential equations:

$$P'(\eta)=A_2\frac{(f')^2}{\eta+k}, \tag{2.19}$$

$$\frac{1}{A_2}\left(\frac{2k}{\eta+k}\right)P=\frac{A_1}{A_2}\left(f'''+\frac{1}{\eta+k}f''-\frac{1}{(\eta+k)^2}f'\right)$$
$$-\frac{k}{\eta+k}\left(f'^2-ff''-\frac{ff'}{\eta+k}\right)+\frac{\beta}{A_2}\frac{k}{\eta+k}\left(g'^2-gg''-\frac{gg'}{\eta+k}\right), \tag{2.20}$$

$$Pr_M\frac{k}{\eta+k}(f''g-fg'')-Pr_M\frac{k}{(\eta+k)^2}(f'g-fg')g'''+\frac{g''}{\eta+k}-\frac{g'}{(\eta+k)^2}, \tag{2.21}$$

$$\frac{A_4}{PrA_3}\left(1+\frac{Rd}{A_4}\right)\left(\theta''+\frac{\theta'}{\eta+k}\right)+\frac{D}{A_3}\theta=\frac{-k}{\eta+k}f\theta', \tag{2.22}$$

$$\frac{1}{Sc}\left(G''+\frac{G'}{\eta+k}\right)+\frac{k}{\eta+k}fG'-\tau_1GH^2=0, \tag{2.23}$$

$$\frac{\delta}{Sc}\left(H''+\frac{H'}{\eta+k}\right)+\frac{k}{\eta+k}fH'+\tau_1GH^2=0, \tag{2.24}$$

subject to the corresponding boundary conditions

$$f(0)=S+sgn(S)h\beta\left(g'(0)\right)^2,\ f'(0)=1, \tag{2.25}$$

$$\theta(0)=1,\ g(0)=0,\ g''(0)=0, \tag{2.26}$$

$$G'(0)=\tau_2G(0),\ \delta H'(0)=-\tau_2G(0), \tag{2.27}$$

$$f'(\infty)\to 0,\ f''(\infty)\to 0,\ \theta(\infty)\to 0, \tag{2.28}$$

$$g'(\infty)\to 1,\ G(\infty)\to 1,\ H(\infty)\to 0. \tag{2.29}$$

Here, the dimensionless parameters are

$$Pr=\vartheta_f(\rho c_p)_f/\kappa_f,\ R_d=16\sigma^*T_\infty^3/3K^*\kappa_f,$$

$$k=R\sqrt{\frac{a}{\vartheta_f}},\ \beta=\frac{\mu_{ef}}{4\pi\rho_f}(\frac{M_0}{a})^2,\ Pr_M=\frac{\vartheta_f}{\zeta},\ D=\frac{Q}{\left(\rho C_p\right)_f a},\ Sc=\frac{\vartheta_f}{D_A},$$

$$\tau_1=\frac{\tau_c C_0^{\ 2}}{a},\ \tau_2=\frac{\tau_s}{D_A}\sqrt{\frac{\vartheta_f}{a}},\ \delta=\frac{D_B}{D_A},\ S=\frac{s_0}{\sqrt{a\vartheta_f}},\ h=\frac{h_0}{A_2\sqrt{a\vartheta_f}}.$$

It's worth noting that the diffusion coefficients D_A and D_B here are equal for both chemical species, *i.e.* $\delta=1$ and, thus

$$G(\eta)+H(\eta)=1, \tag{2.30}$$

Then, Equations (2.23) and (2.24) yield

$$\frac{1}{Sc}\left(G''+\frac{G'}{\eta+k}\right)+\frac{k}{\eta+k}fG'-\tau_1G(1-G)^2=0, \tag{2.31}$$

with the boundary conditions

$$G'(0)=\tau_2G(0),\ G(\infty)\to 1. \tag{2.32}$$

Furthermore, by differentiating Equation (2.20) and using Equation (2.19) to eliminate pressure from the momentum equation, we ultimately arrive at the task of solving the following system of nonlinear coupled ordinary differential equations:

$$f^{iv}+\frac{2f'''}{\eta+k}-\frac{f''}{(\eta+k)^2}+\frac{f'}{(\eta+k)^3}$$
$$+\frac{A_2}{A_1}\left[\left(\frac{k}{\eta+k}\right)(ff'''-ff'')+\left(\frac{k}{(\eta+k)^2}\right)(ff''-f'^2)-\left(\frac{k}{(\eta+k)^3}\right)ff'\right] \quad (2.33)$$
$$+\frac{\beta}{A_1}\frac{k}{(\eta+k)}\left(g'g''-gg'''+\frac{gg'}{(\eta+k)^2}-\frac{g'^2+gg''}{\eta+k}\right)=0.$$

$$Pr_M\frac{k}{\eta+k}(f''g-fg'')-Pr_M\frac{k}{(\eta+k)^2}(f'g-fg')=g'''+\frac{g''}{\eta+k}-\frac{g'}{(\eta+k)^2}, \quad (2.34)$$

$$\frac{A_4}{PrA_3}\left(1+\frac{Rd}{A_4}\right)\left(\theta''+\frac{\theta'}{\eta+k}\right)+\frac{D}{A_3}\theta=\frac{-k}{\eta+k}f\theta', \quad (2.35)$$

$$\frac{1}{Sc}\left(G''+\frac{G'}{\eta+k}\right)+\frac{k}{\eta+k}fG'-\tau_1G(1-G)^2=0, \quad (2.36)$$

incorporating the boundary conditions

$$f(0)=S+sgn(S)h\beta(g'(0))^2,\ \ f'(0)=1, \quad (2.37)$$

$$\theta(0)=1,\ \ g(0)=0,\ \ g''(0)=0,\ \ G'(0)=\tau_2G(0), \quad (2.38)$$

$$f'(\infty)\to 0,\ \ f''(\infty)\to 0,\ \ \theta(\infty)\to 0, \quad (2.39)$$

$$g'(\infty)\to 1,\ \ G(\infty)\to 1,\ \ H(\infty)\to 0. \quad (2.40)$$

2.4. The Physical Quantities

The critical measurable parameters of interest, namely the surface shear stress C_f and the Nusselt number Nu, which quantifies the heat flux rate at the surface, are expressed as follows:

$$C_f=\frac{\mu_{hnf}\left(\frac{\partial u}{\partial r}-\frac{u}{r+R}\right)_{r=0}}{\rho_{hnf}(as)^2},\ \ Nu=\frac{s\left(-\kappa_{hnf}\left.\frac{\partial T}{\partial r}\right|_{r=0}-\frac{16\sigma^*T_\infty^{\ 3}}{3K^*}\left.\frac{\partial T}{\partial r}\right|_{r=0}\right)}{\kappa_f(T_w-T_\infty)}. \quad (2.34)$$

The expressions given in Equation (2.34), when transformations from Equations (2.15)-(2.17) are applied, can be rewritten as

$$C_fRe_s^{1/2}=\frac{A_1}{A_2}\left(f''(0)-\frac{f'(0)}{k}\right). \quad (2.35)$$

$$NuRe_s^{-1/2}=-(A_4+R_d)\theta'(0). \quad (2.36)$$

where $Re_s=as^2/\vartheta_f$ is the local Reynolds number.

3. Numerical Solution

In this section, we choose water as the base fluid, a substance commonly selected for its heat transfer capabilities. Copper (Cu) and multi-walled carbon nanotubes

(MWCNTs) are employed as two different types of magnetic nanoparticles to be added to the base fluid, resulting in the formation of a hybrid nanofluid. The associated thermophysical properties of both the base fluid and the nanoparticles are presented in **Table 2**.

Employing an improved shooting method, augmented with Runge-Kutta and Newton's iterative techniques as detailed in [24], we numerically solve the nonlinear governing Equations (2.23) to (2.26), accompanied by the boundary conditions (2.37 - 2.40). The comparison of our results with the published data shows a high level of agreement, as shown in **Table 3**, which confirms the accuracy of our method.

Table 2. Thermophysical properties of the base fluid and nanoparticles.

Material	ρ (kg/m^3)	C_p (J/kg·K)	κ (W/m·K)
Water (Base fluid)	997.1	4179	0.613
Cu (Nanoparticles)	8933	385	400
MWCNTs (Nanoparticles)	1600	796	3000

Table 3. Comparison of $-C_f Re_s^{1/2}$ with different values of curvature parameter. $S = 0$, $\beta = 0$, $\Phi_1 = \Phi_2 = 0$.

k	Rosca *et al.* [25]	Present Results
5	1.15076	1.15076
10	1.07172	1.07349
20	1.03501	1.03561
30	1.02315	1.02353
40	1.01729	1.01759

4. Results and Discussion

For the convenience of analysis, the following parameter values are chosen in the analysis unless otherwise stated: $R_d = 10$, $Sc = 0.1$, $\Phi_1 = \Phi_2 = 0.01$, $Pr_M = 0.1$, $Pr = 2$, $h = 10$, $\tau_1 = \tau_2 = 0.5$, $k = 10$, $D = 0.1$, $S = 0.5$.

4.1. Velocity Profiles

Figure 2 presents the velocity profiles as the curvature radius parameter k varies. It is evident that with the increase of k, both the nanofluid and hybrid nanofluid velocity profiles exhibit an upward trend. This trend is primarily due to the fact that as the parameter k increases, the centrifugal force acting on the fluid during flow also intensifies, thereby promoting an increase in velocity. The influence of parameters β and h on velocity is depicted in **Figure 3** and **Figure 4**. It is observed that in both hybrid nanofluid and nanofluid scenarios, the velocity decreases as β and h increase. Notably, the hybrid nanofluid is more responsive to changes in β, while the nanofluid is more sensitive to variations in h.

4.2. Temperature and Concentration Profiles

Figure 5 displays the temperature profiles as k varies. It is evident that with an increase in k, the temperature profiles for both nanofluid and hybrid nanofluid show a decreasing trend. Notably, the sensitivity of both nanofluids to this parameter is almost identical. **Figure 6** delineates the influence of parameter Pr_M on temperature profiles. With the augmentation of Pr_M, the temperature of both nanofluid and hybrid nanofluid increases. Moreover, the hybrid nanofluid demonstrates greater effectiveness.

As the parameter k increases, the trend of concentration for both nanofluids and hybrid nanofluids exhibits an inverse relationship with temperature, as shown in **Figure 7**. Significantly, a higher value of k corresponds to greater concentrations in these fluids.

Figure 8 shows that higher homogeneous parameter values τ_1 lead to lower concentrations due to reactant consumption. **Figure 9** mirrors this trend for the heterogeneous parameter τ_2, where increasing τ_2 also reduces concentration, aligning with typical reaction dynamics.

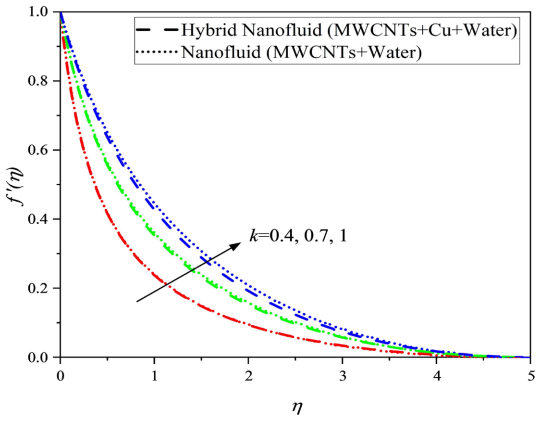

Figure 2. Impact of k on velocity $f'(\eta)$ for hybrid nanofluid and nanofluid.

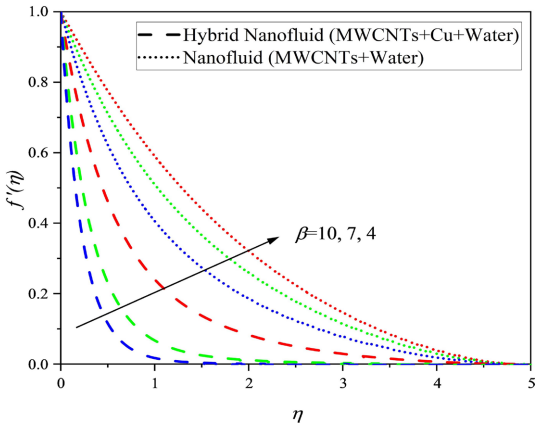

Figure 3. Impact of β on $f'(\eta)$ for hybrid nanofluid and nanofluid.

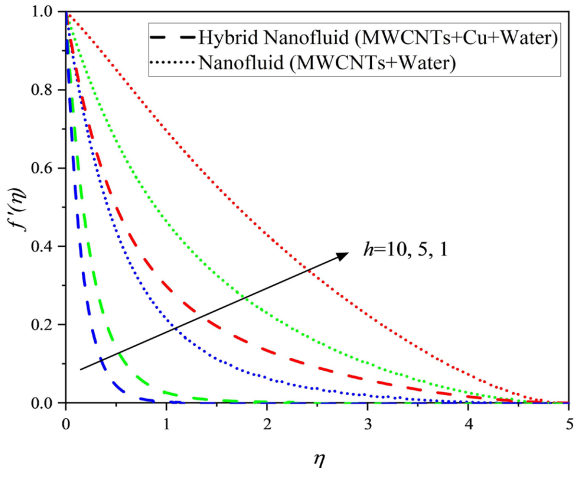

Figure 4. Impact of h on $f'(\eta)$ for hybrid nanofluid and nanofluid when $S = 20$.

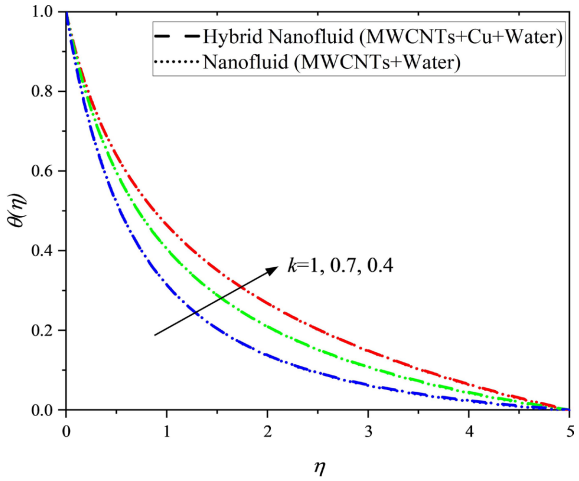

Figure 5. Impact of k on $\theta(\eta)$ for hybrid nanofluid and nanofluid.

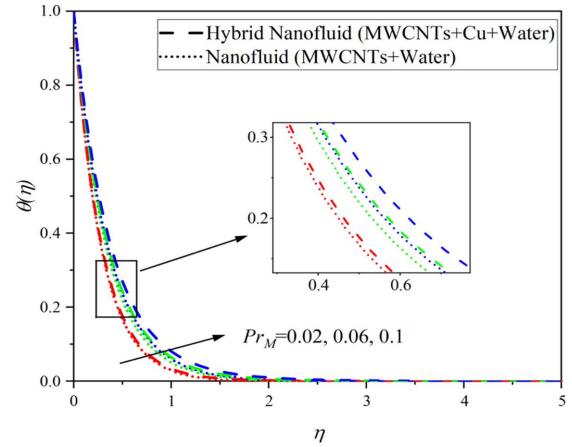

Figure 6. Impact of Pr_M on $\theta(\eta)$ for hybrid nanofluid and nanofluid.

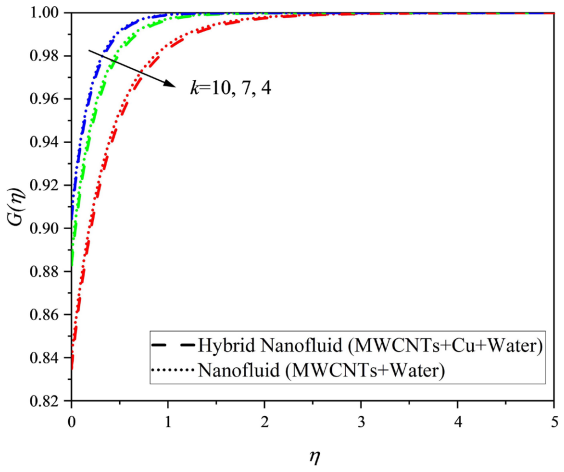

Figure 7. Impact of k on $G(\eta)$ for hybrid nanofluid and nanofluid when $D = 10$.

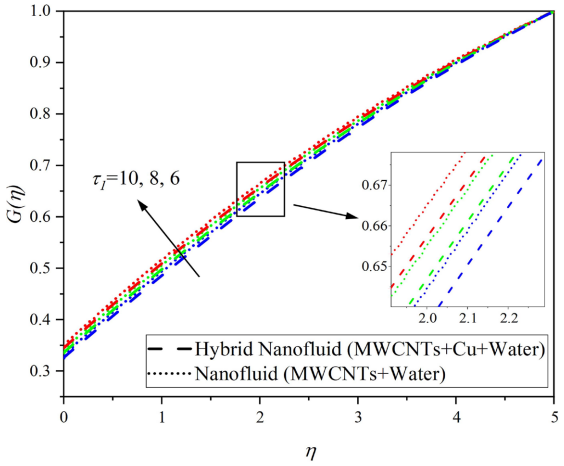

Figure 8. Impact of τ_1 on $G(\eta)$ for hybrid nanofluid and nanofluid when $k = 50$, $Sc = 0.013$.

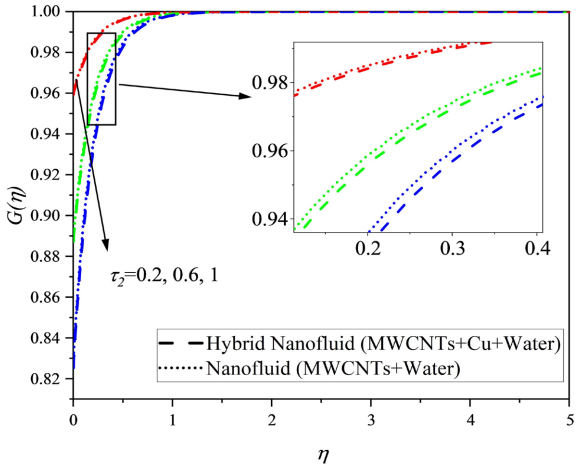

Figure 9. Impact of τ_2 on $G(\eta)$ for hybrid nanofluid and nanofluid.

4.3. Effect of Governing Parameters on Skin Friction Coefficient and Nusselt Number

Figure 10 illustrates the effect of the dimensionless curvature radius parameter k on the surface friction coefficient for a hybrid nanofluid. It is evident that increasing the value of k (*i.e.*, reducing the dimensionless curvature) leads to an increase in the magnitude of surface friction on the sheet. Consequently, on the surface of the stretching sheet, more force is required to drag fluid over a flat surface compared to a curved one. It is clear from **Figure 11** that the magnitude of the skin friction coefficient increases for hybrid nanofluid with enhanced suction s, which aligns with physical fact. Furthermore, it is found in **Figure 10** and **Figure 11** that the variation of D and Rd do not affect the surface friction force, which is consistent with Equations (2.33)-(2.36), further confirming the validity of the results.

Figure 12 demonstrates that an increase in the value of k for hybrid nanofluid leads to a slight increase in the Nusselt number. On surfaces with lower curvature, the boundary layer develops more readily because the centrifugal forces acting on the fluid flow are reduced, which in turn enhances heat transfer within the boundary layer. However, an opposite trend is observed where the Nusselt number decreases with the increase of D. **Figure 13** reveals that an augment in Rd *and* s leads to an increase in the Nusselt number for hybrid nanofluid, indicating a significant enhancement in convective heat transfer efficiency.

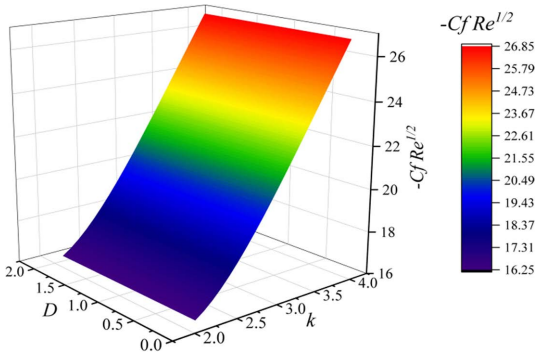

Figure 10. Impact of k and D on the surface friction coefficient for hybrid nanofluid when $S = 3$.

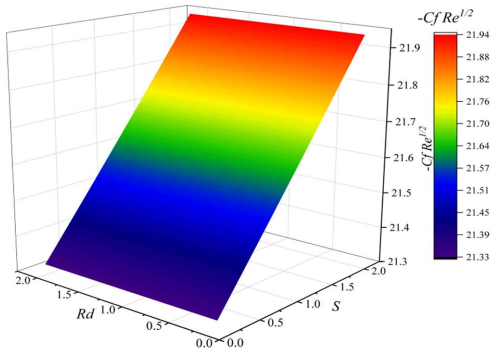

Figure 11. Impact of Rd and S on $G(\eta)$ on the surface friction coefficient for hybrid nanofluid when $k = 1$.

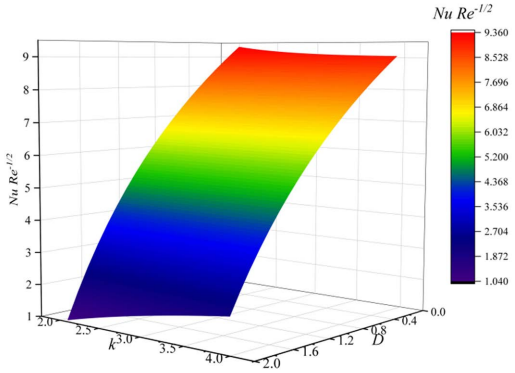

Figure 12. Impact of k and D on the Nusselt number for hybrid nanofluid when $S = 3$.

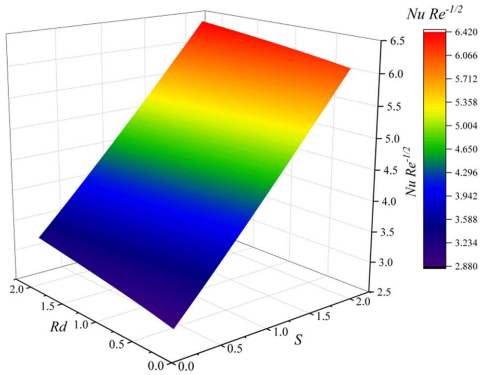

Figure 13. Impact of Rd and S on $G(\eta)$ onthe Nusselt number for hybrid nanofluid.

5. Conclusions

Conducting a numerical study on the flow of hybrid nanofluid over a stretching curved surface, we have arrived at the following main findings.

1) Fluid velocity increases with the curvature radius parameter k due to stronger centrifugal forces.

2) The increase in β and h decreases fluid velocity, with hybrid nanofluids being more sensitive to β and nanofluids to h.

3) As k increases, fluid temperature decreases while concentration increases.

4) The augmentation of τ_1 and τ_2 yields a concomitant decrease in concentration attributable to reactant consumption.

5) The surface friction coefficient increases with k, s, indicating greater force is needed to drag the fluid over a stretching surface.

6) The Nusselt number increases with k, Rd and s, indicating an improvement in convective heat transfer efficiency.

In summary, this study provides an understanding of fluid dynamics, heat and mass transfer of hybrid nanofluids under complex flow conditions and offers strategies for optimizing heat transfer processes in industrial applications.

Funding

This research was funded by the Natural Science Foundations of Fujian Province, Grant 2023J01415.

Conflicts of Interest

The authors declare no conflicts of interest regarding the publication of this paper.

References

[1] Tembhare, S.P., Barai, D.P. and Bhanvase, B.A. (2022) Performance Evaluation of Nanofluids in Solar Thermal and Solar Photovoltaic Systems: A Comprehensive Review. *Renewable and Sustainable Energy Reviews*, **153**, Article ID: 111738. https://doi.org/10.1016/j.rser.2021.111738

[2] Mukherjee, S., Ebrahim, S., Mishra, P.C., Ali, N. and Chaudhuri, P. (2022) A Review on Pool and Flow Boiling Enhancement Using Nanofluids: Nuclear Reactor Application. *Processes*, **10**, Article No. 177. https://doi.org/10.3390/pr10010177

[3] Choil, S.U.S. and Eastman, J.A. (1995) Enhancing Thermal Conductivity of Fluids with Nanoparticles. Argonne National Laboratory. https://digital.library.unt.edu/ark:/67531/metadc671104

[4] Jones-Jackson, S., Rodriguez, R., Yang, Y., Lopera, L. and Emadi, A. (2022) Overview of Current Thermal Management of Automotive Power Electronics for Traction Purposes and Future Directions. *IEEE Transactions on Transportation Electrification*, **8**, 2412-2428. https://doi.org/10.1109/tte.2022.3147976

[5] Kalsi, S., Kumar, S., Kumar, A., Alam, T. and Dobrotă, D. (2023) Thermophysical Properties of Nanofluids and Their Potential Applications in Heat Transfer Enhancement: A Review. *Arabian Journal of Chemistry*, **16**, Article ID: 105272. https://doi.org/10.1016/j.arabjc.2023.105272

[6] Muhammad, K., Hayat, T., Alsaedi, A., Ahmad, B. and Momani, S. (2020) Mixed Convective Slip Flow of Hybrid Nanofluid (Mwcnts + Cu + Water), Nanofluid (Mwcnts + Water) and Base Fluid (Water): A Comparative Investigation. *Journal of Thermal Analysis and Calorimetry*, **143**, 1523-1536. https://doi.org/10.1007/s10973-020-09577-z

[7] Abbas, N., Rehman, K.U., Shatanawi, W. and Malik, M.Y. (2022) Numerical Study of Heat Transfer in Hybrid Nanofluid Flow over Permeable Nonlinear Stretching Curved Surface with Thermal Slip. *International Communications in Heat and Mass Transfer*, **135**, Article ID: 106107. https://doi.org/10.1016/j.icheatmasstransfer.2022.106107

[8] Sanni, K.M., Saliu, A. and Asghar, S. (2024) Heat and Mass Transport of an Advection-Diffusion Viscous Fluid Past a Magnetized Multi-Physical Curved Stretching Sheet with Chemical Reaction. *Mathematical and Computer Modelling of Dynamical Systems*, **30**, 131-155. https://doi.org/10.1080/13873954.2024.2311392

[9] Waqas, H., Bukhari, F.F., Farooq, U., Alqarni, M.S. and Muhammad, T. (2021) Numerical Computation of Melting Heat Transfer in Nonlinear Radiative Flow of Hybrid Nanofluids Due to Permeable Stretching Curved Surface. *Case Studies in Thermal Engineering*, **27**, Article ID: 101348. https://doi.org/10.1016/j.csite.2021.101348

[10] Chaudhary, M.A. and Merkin, J.H. (1995) A Simple Isothermal Model for Homogeneous-Heterogeneous Reactions in Boundary-Layer Flow. I Equal Diffusivities. *Fluid Dynamics Research*, **16**, 311-333. https://doi.org/10.1016/0169-5983(95)00015-6

[11] Chaudhary, M.A. and Merkin, J.H. (1995) A Simple Isothermal Model for Homogeneous-Heterogeneous Reactions in Boundary-Layer Flow. II Different Diffusivities for Reactant and Autocatalyst. *Fluid Dynamics Research*, **16**, 335-359. https://doi.org/10.1016/0169-5983(95)90813-h

[12] Ullah, I. and Xu, Y. (2025) Computational Study of Homogeneous-Heterogeneous Reactions in Bioconvective Third-Grade Material Flow. *Journal of Computational and Applied Mathematics*, **454**, Article ID: 116181. https://doi.org/10.1016/j.cam.2024.116181

[13] Gangadhar, K., Prameela, M., Chamkha, A.J., G R, B. and Kannan, T. (2024) Evaluation of Homogeneous-Heterogeneous Chemical Response on Maxwell-Fluid Flow through Spiraling Disks with Nonlinear Thermal Radiation Using Numerical and Regularized Machine Learning Methods. *International Journal of Modelling and Simulation*. https://doi.org/10.1080/02286203.2024.2327598

[14] Imtiaz, M., Mabood, F., Hayat, T. and Alsaedi, A. (2019) Homogeneous-Heterogeneous Reactions in MHD Radiative Flow of Second Grade Fluid Due to a Curved Stretching Surface. *International Journal of Heat and Mass Transfer*, **145**, Article ID: 118781. https://doi.org/10.1016/j.ijheatmasstransfer.2019.118781

[15] Javed, M., Qadeer, F., Imran, N., Kumam, P. and Sohail, M. (2022) Peristaltic Mechanism of Ellis Fluid in Curved Configuration with Homogeneous and Heterogeneous Effects. *Alexandria Engineering Journal*, **61**, 10677-10688. https://doi.org/10.1016/j.aej.2022.03.065

[16] Sanni, K.M., Hussain, Q. and Asghar, S. (2021) Flow of Magnetohydrodynamic Viscous Fluid by Curved Configuration with Non-Linear Boundary Driven Velocity. *Journal of Taibah University for Science*, **15**, 589-598. https://doi.org/10.1080/16583655.2021.1991076

[17] Sanni, K., Adediran, A. and Tajudeen, A. (2023) Numerical Investigation of Nonlinear Radiative Flux of Non-Newtonian MHD Fluid Induced by Nonlinear Driven Multi-Physical Curved Mechanism with Variable Magnetic Field. *Journal of the Nigerian Society of Physical Sciences*, **5**, 1435. https://doi.org/10.46481/jnsps.2023.1435

[18] Sheng, Z., Ding, Y., Li, G., Fu, C., Hou, Y., Lyu, J., *et al.* (2021) Solid-Liquid Host-guest Composites: The Marriage of Porous Solids and Functional Liquids. *Advanced Materials*, **33**, Article ID: 2104851. https://doi.org/10.1002/adma.202104851

[19] Sheng, Z., Wang, H., Tang, Y., Wang, M., Huang, L., Min, L., *et al.* (2018) Liquid Gating Elastomeric Porous System with Dynamically Controllable Gas/Liquid Transport. *Science Advances*, **4**, eaao6724. https://doi.org/10.1126/sciadv.aao6724

[20] Chen, B., Zhang, R., Hou, Y., Zhang, J., Chen, S., Han, Y., *et al.* (2021) Light-Responsive and Corrosion-Resistant Gas Valve with Non-Thermal Effective Liquid-Gating Positional Flow Control. *Light*: *Science & Applications*, **10**, Article No. 127. https://doi.org/10.1038/s41377-021-00568-9

[21] Chen, H., Ma, Y., Shen, M., He, P. and Zhang, H. (2023) Significance of Cattaneo-Christov Double Diffusion and Induced Magnetic Field on Maxwell Ternary Nanofluid Flow with Magnetic Response Boundary. *Journal of Magnetism and Magnetic Materials*, **587**, Article ID: 171264. https://doi.org/10.1016/j.jmmm.2023.171264

[22] Abdul Hakeem, A.K. and Sathiyanathan, K. (2009) An Analytic Solution of an Oscillatory Flow through a Porous Medium with Radiation Effect. *Nonlinear Analysis*: *Hybrid Systems*, **3**, 288-295. https://doi.org/10.1016/j.nahs.2009.01.011

[23] Imtiaz, M., Mabood, F., Hayat, T. and Alsaedi, A. (2019) Homogeneous-Heterogeneous Reactions in MHD Radiative Flow of Second Grade Fluid Due to a Curved

Stretching Surface. *International Journal of Heat and Mass Transfer*, **145**, Article ID: 118781. https://doi.org/10.1016/j.ijheatmasstransfer.2019.118781

[24] Zheng, L., Liang, C. and Zhang, X. (2007) A Numerical Method for Solving the Boundary Layer Equations of Laminar Natural Convention about a Vertical Plate. *Journal of University of Science and Technology Beijing*, *Mineral*, *Metallurgy*, *Material*, **14**, 33-35. https://doi.org/10.1016/s1005-8850(07)60007-3

[25] Roşca, N.C. and Pop, I. (2015) Unsteady Boundary Layer Flow over a Permeable Curved Stretching/Shrinking Surface. *European Journal of Mechanics-B/Fluids*, **51**, 61-67. https://doi.org/10.1016/j.euromechflu.2015.01.001